Journal of Applied Fluid Mechanics, Vol. 18, No. 1, pp. 131-144, 2025.
Available online at www.jafmonline.net, ISSN 1735-3572, EISSN 1735-3645.
https://doi.org/10.47176/jafm.18.1.2758

Effect of the Circumferential Position of Balance Holes on the Cavitation Performance and Cavitation Erosion of Centrifugal Pump

D. Xun[1], N. Qiu[1†], Y. Wei[1], H. Zhu[1], W. Zhou[2], P. Xu[1] and W. Zhang[3]

[1] *Research Center of Fluid Machinery Engineering and Technology, Jiangsu University, Zhenjiang, 212013, China*
[2] *School of Energy and Power Engineering, Jiangsu University, Zhenjiang, 212013, China*
[3] *Key Laboratory of Fluid and Power Machinery (Xihua University), Ministry of Education, Chengdu, 610039, China*

†Corresponding Author Email: qiuning@ujs.edu.cn

ABSTRACT

The flow field of a low specific speed centrifugal pump is investigated in the present work based on numerical simulation to establish the effect of circumferential positions of balance holes on cavitation behaviour and cavitation erosion of the centrifugal pump. The distribution of the pressure around balance holes is studied, the initiation and development of cavitation at different balance hole schemes are compared, and the distribution of cavitation erosion for the original pump and the ideal scheme is also predicted. The results show that when the NPSHa is high, there is low pressure zone in balance hole, which leads to cavitation in the pump. The cavitation performance of pump is improved by gradually moving balance holes away from blade suction surface, as this reduces low pressure zones around the balance hole and incipient cavitation. Under critical cavitation conditions, the cavitation shows a tendency to collapse as the angle (φ) of circumferential position of balance holes decreases, and the proportion of the higher vapor volume fraction in cavitation core zones also decreases. The cavitation erosion zones on blade surfaces are predicted by using the Erosive Power Method (EPM). The erosion impact of the original pump is more pronounced in the comparative results.

Article History

Received April 2, 2024
Revised June 17, 2024
Accepted August 1, 2024
Available online November 6, 2024

Keywords:

Centrifugal pump
Balance hole
Circumferential position of balance hole
Cavitation erosion
The Erosive Power Method (EPM)

1. INTRODUCTION

Cavitation is the process of bubbles formation and collapse that occur when the local pressure drops below the vapor pressure at the corresponding condition during the operation of fluid machines (Haosheng et al., 2008; Brennen, 2011). The collapse of cavitation can cause a load impact on the blade surface (Melissaris et al., 2020). Long-term operation under cavitation conditions could lead to erosion pits forming on the blade surface (Zhu et al., 2021; Chen et al., 2022). This would not only compromise the safety and stability of the pump but also drastically diminish its service life (Aktas et al., 2018; Wang et al., 2018).

In engineering technology and scientific research, the cavitation behaviour curve is typically an important tool for assessing the cavitation behaviour of centrifugal pumps, which is characterized by a sharp decline under critical cavitation conditions (at 3% head loss) (Gao et al., 2017; Zhang et al., 2018). Low specific speed centrifugal pumps have narrow flow passages, and when cavitation occurs, the bubbles quickly obstruct the flow passages, resulting in degraded pump performance (Cui et al., 2020; Zhao et al., 2020; Gangipamula et al., 2022). Based on this context, it is crucial for engineering applications and scientific research to enhance the cavitation behaviour of pumps, primarily by preventing cavitation inception and delaying the development of cavitation. The impact mechanism of different design parameters on cavitation has been researched and compared to enhance the cavitation behaviour of pumps (Luo et al., 2016; Huang et al., 2018). Hu et al. (2020) examined the impact of inlet angle of attack on cavitation of a pump and compared three different inlet angles of attack, 8°, 0°, and -8°, and discovered that the flow uniformity could be effectively improved with a positive inlet angle of attack (8°). Luo et al. (2008) explored cavitation behaviour of boiler feed pumps based on the VOF cavitation model. They found that increasing blade inlet angle can efficiently enhanced its cavitation behaviour. Zhu and Chen (2012) examined the cavitation behaviour of pumps and discovered that the addition of a tiny blade in the front position of blade may effectively prevent its cavitation. Despite the fact that a number of cavitation improvement methods have been presented, the alterations to the construction of pump are

large, the implementation process is complicated, and the influence on head and efficiency is still unknown.

This work investigates cavitation under different schemes by changing angle of balance hole with horizontal line, thus exploring feasible methods to control cavitation. The balance hole can be utilized to counterbalance the axial thrust force between shroud and hub of the impeller that is generated by the pressure difference. Zhao et al. (2012) examined the effect of different balance hole radial positions in the hub on balancing the axial force. They discovered that the pressure inside balance holes increased as radial radius increased, as did the axial force. Luo et al. (2022) compared the effect of balance holes arrangement position on the axial force of an impeller on the basis of the two-phase condition, the findings revealed that the axial force increases as the radial positions increases and decreases as the balance hole diameter increases. Cao et al. (2022) observed that as the size of balance hole increased, the critical cavitation number decreased, and pressure within the mechanical seal steadily decreases. Cheng et al. (2020) made a analysis and comparison of differences in cavitation behaviour under different balance holes ratio area schemes, and it was discovered that the flow conditions in the pump were severely compromised once the ratio area reached a certain value. Wang et al. (2021) researched cavitation behaviour of balance holes under varying radial positions by combining experiments and simulations. By comparison they point out that critical cavitation number reduced before rising with increasing radial locations of the balance hole.

There are many scholars who have conducted further studies on the issue of cavitation erosion. Dular et al. (2006) proposed a new cavitation erosion method on the basis of relationship between the standard deviation of the vapor fraction and erosion energy. The calculations of the method correlates well with that of their erosion experiments. Li et al. (2014) used hydrofoils as a research carrier and suggested a method based on solving the wall surface pressure time derivative for predicting the emergence and growth of cavitation erosion. Usta and Korkut (2019) combined the flow characteristics of the fluid with the damaged area of the surface and proposed the pre-diction method of the Erosive Power Method, which was successfully applied to the study of hydrofoils and propellers. Koksal et al. (2021) obtained erosion intensity of propeller surfaces by employing the Erosive Power Method, while the erosion characteristics obtained from the simulations agreed well with the experimental datas. Li et al. (2021) developed a multiscale model theory based on VOF method and DBM as well as used the very large eddy simulation to capture more accurate features of the cavitation flow field, laying a foundation for predicting cavitation erosion. Arabnejad et al. (2021) used the erosion prediction theory on the basis of kinetic energy of liquid around collapsed structure to predict erosion regions in a nozzle, and predicted results were strongly correlated with the test zones. Wang et al. (2022) researched the cavitation flow field surrounding the Delft Twist-11 hydrofoil by adopting the LES and calculated erosion intensity on this hydrofoil surface employing the energy balance approach (EBA). The erosion zones of calculated results of simulation agreed well with the experiment. Accurately capturing the multiscale cavitation characteristics using the Eulerian-Lagrangian method is essential for accurately predicting erosion zones and intensity. Wang et al. (2023) and Li et al. (2024) employed this approach to predict erosion on a twisted hydrofoil surface and their findings demonstrated efficient predictive abilities.

Currently, the mechanism of cavitation erosion is very complex and unknown, and there are limited theoretical study on the impact of balance hole positions on cavitation erosion. The research object of this work is a centrifugal pump with balance holes, the location of balance holes is changed along the circumferential direction. The internal flow field information are captured by numerical method. And the cavitation erosion zones and intensity on the blade surfaces are calculated by following the Erosive Power Method (EPM). In addition, the differences and influencing mechanism of cavitation behaviour as well as cavitation erosion of this pump with different circumferential position schemes are compared. Finally, a balance hole position scheme with good cavitation performance is proposed, which provides essential theoretical support for further in-depth study on impact of the balance holes on cavitation performance and cavitation erosion mechanism of centrifugal pumps and practical engineering applications.

2. EXPERIMENTAL METHODOLOGY

2.1 Centrifugal Pump Parameters

The ZA20-250 low specific speed centrifugal pump is investigated in this work. The design flow rate Q_d, design rotate speed n, and design head H_d of this pump are 10 m^3/h, 2900 rpm, and 80 m, respectively. And the specific speed n_s calculated by formula ($3.65\ (n\sqrt{Q_d}/{H_d}^{3/4})$) is 21. The experiment employed water as the medium, its density and dynamic viscosity are 998.9 kg/m^3 and 0.00101 Pa·s. The other parameters are listed in Table 1. The full flow field model is used in the simulation to obtain more realistic flow field simulation results, including the balance hole and wear ring. Figure 1 shows the computational domain employed for the simulation.

2.2 The Design Scheme for the Circumferential Positions of Balance Holes

A schematic representation of positions of the balance holes is shown in Fig. 2. The angle between the center of balance hole and horizontal line is denoted by φ. The φ of the original pump is 50°, and the location of the balance hole is changed by varying the size of φ. In this work,

Table 1 Detailed parameters of the mode pump

Parameters	Value
Number of blades (Z)	3
Impeller outlet width (b_2)	6.5 mm
Impeller diameter (D_2)	259 mm
Outlet pipe diameter (D_d)	25 mm
Inlet pipe diameter (D_s)	50 mm
Blades wrap angle (β)	190°

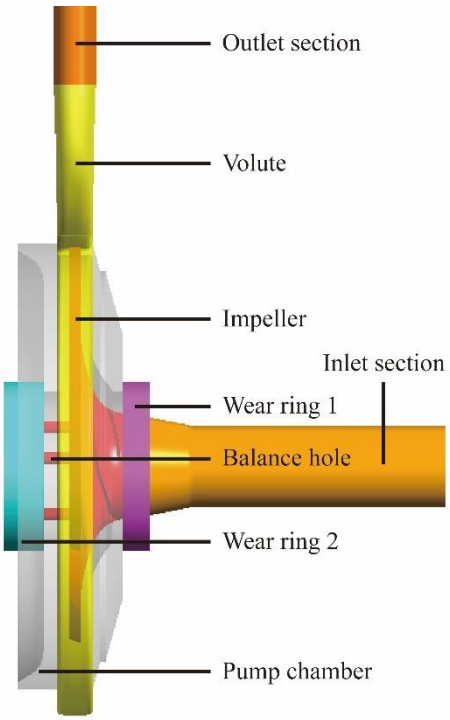

Fig. 1 Three-dimensional structure of the full flow field of the centrifugal pump

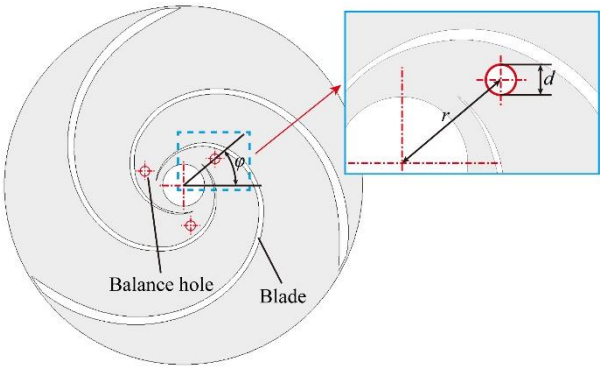

Fig. 2 Position of the balance holes

Table 2 Parameters of the balance hole rotation scheme

Scheme	φ (°)	d (mm)	r (mm)
Original	50	7	30
I	40	7	30
II	30	7	30
III	20	7	30

three rotation schemes are designed for balance hole which rotates by 10° clockwise while the hole diameter d and the radial radius r remain unchanged. The particular parameters for each scheme is shown in Table 2.

2.3 Experimental Setup

The experiment is conducted at the Research Center of Fluid Machinery Engineering and Technology of Jiangsu University. The structure of the closed test bench is shown in Fig. 3 (Wei et al., 2021). The test system

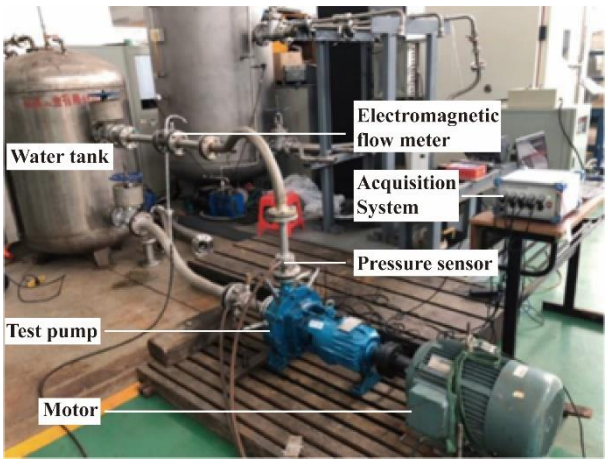

Fig. 3 Test bench structure (Wei et al., 2021)

includes a water circulation loop and a data collection system, which mainly consists of the motor, electromagnetic flowmeter, gate valve, pressure sensor, and centrifugal pump, respectively. In this experiment, the valve on outlet pipeline of this equipment may be changed to control the flow rate, and real-time flow rate data is collected using an electromagnetic flowmeter. Pressure sensors are positioned on both the inlet and outlet pipelines to measure pressure.

3. NUMERICAL METHODOLOGY

3.1 Governing Equations

In this study, the continuity and momentum equations on the basis of the Navier-Stokes equations applied are described as follows (Peters et al., 2015; Yin et al., 2021),

$$\frac{\partial \rho_m}{\partial t}+\frac{\partial(\rho_m u_i)}{\partial x_i}=0 \tag{1}$$

$$\frac{\partial(\rho_m u_i)}{\partial t}+\frac{\partial(\rho_m u_i u_j)}{\partial x_j}=-\frac{\partial p}{\partial x_i}+\frac{\partial}{\partial x_j}\left[(\mu_m+\mu_t)\left(\frac{\partial u_i}{\partial x_j}+\frac{\partial u_j}{\partial x_i}\right)\right] \tag{2}$$

where t, u, p and μ_t are the time variable, velocity, local pressure and turbulent viscosity, respectively. The density of the mixture fluid ρ_m and the mixed dynamic viscosity μ_m are defined as,

$$\rho_m=\rho_l\alpha_l+\rho_v\alpha_v \tag{3}$$

$$\mu_m=\mu_l\alpha_l+\mu_v\alpha_v \tag{4}$$

$$\alpha_v+\alpha_l=1 \tag{5}$$

where ρ_l and ρ_v, α_l and α_v, μ_l and μ_v represent the density, volume fraction and dynamic viscosity of gas phase and liquid phase, respectively.

3.2 Cavitation Model

This work employs the Zwart model (Zwart et al., 2004) for cavitation mass transfer, which defines the cavitation evolution process on account of transport

relationship between liquid and gas phases, which can be defined as,

$$\frac{\partial(\rho_v\alpha_v)}{\partial t}+\frac{\partial(\rho_v\alpha_v u_i)}{\partial x_i}=\dot{m}^+-\dot{m}^- \tag{6}$$

$$\dot{m}^+=3\alpha_{nuc}C_1\frac{(1-\alpha_v)\rho_v}{R_B}\sqrt{\frac{2(p_v-p)}{3\rho_l}},\ p<p_v \tag{7}$$

$$\dot{m}^-=3C_2\frac{\alpha_v\rho_v}{R_B}\sqrt{\frac{2(p-p_v)}{3\rho_l}},\ p\geq p_v \tag{8}$$

where $\dot{m}^+$ and $\dot{m}^-$ are evaporation and condensation rates, α_{nuc} represents the vapor core volume fraction, C_1 and C_2 are evaporation and condensation coefficients, R_B is cavitation bubble radius. The empirical constants are set to $C_1 = 50$, $C_2 = 0.01$, $R_B = 0.001$ mm, $\alpha_{nuc} = 1\times10^{-4}$.

3.3 Turbulence Model

The flow field inside the pump becomes more complicated due to the presence of the balance hole. To achieve realistic simulation results of the internal flow channel, the SST $k-\omega$ turbulence model (Peters et al., 2015) is chosen for simulation in this work. The model includes a hybrid function that is derived from the regular $k-\omega$ model. The transmission of turbulent shear stress is accounted for in turbulent viscosity, making the SST $k-\omega$ model more accurate and trustworthy. The turbulent kinetic energy equation k, turbulent frequency equation ω and eddy viscosity equation μ_t are expressed as,

$$\frac{\partial(\rho_m k)}{\partial t}+\frac{\partial}{\partial x_j}(\rho_m U_j k)=\frac{\partial}{\partial x_j}\left[\left(\mu_m+\frac{\mu_t}{\sigma_k}\right)\frac{\partial k}{\partial x_j}\right]+P_k-\beta^*\rho_m k\omega \tag{9}$$

$$\frac{\partial(\rho_m\omega)}{\partial t}+\frac{\partial}{\partial x_j}(\rho_m U_j\omega)=\frac{\partial}{\partial x_j}\left[\left(\mu_m+\frac{\mu_t}{\sigma_\omega}\right)\frac{\partial\omega}{\partial x_j}\right]+\alpha\frac{\omega}{k}P_k-\beta\rho_m\omega^2+2(1-F_1)\rho_m\frac{1}{\sigma_{\omega2}\omega}\frac{\partial k}{\partial x_j}\frac{\partial\omega}{\partial x_j} \tag{10}$$

$$\mu_t=\frac{a_1 k}{max(a_1,\omega,SF_2)} \tag{11}$$

where P_k represents the turbulence generation rate, S represents a fixed strain rate estimate, and the constants are set toβ = 0.075, $\sigma_{\omega2}$ = 1/0.856. F_1 and F_2 are hybrid functions which are obtained from,

$$F_1=\tanh\left(\Phi_1^4\right) \tag{12}$$

$$F_2=\tanh\left(\Phi_2^2\right) \tag{13}$$

$$\Phi_1=min\left(max\left(\frac{\sqrt{k}}{\beta\omega y},\frac{500\mu_m}{\rho_m y^2\omega}\right),\frac{4\rho_m k}{\sigma_{\omega2}D_w^+ y^2}\right) \tag{14}$$

$$D_w^+=max\left(2\rho_m\frac{1}{\sigma_{\omega2}\omega}\frac{\partial k}{\partial x_j}\frac{\partial\omega}{\partial x_j},1.0\times10^{-10}\right) \tag{15}$$

$$\Phi_2=max\left(\frac{2\sqrt{k}}{\beta\omega y},\frac{500\mu_m}{\rho_m y^2\omega}\right) \tag{16}$$

where y represents the distance that is closest to the wall.

3.4 Erosion Assessment Method

Under the current conditions, CFD-based methods can effectively capture the macroscopic cavitation structure, but it is challenging to capture the energy shock caused by cavitation bubble collapses, which occurs in a real cavitation flow field, under microscopic conditions. Patella and Reboud (Fortes Patella & Reboud, 1998) defined the potential energy prior to the macroscopic cavitation structure collapsing as,

$$E_{pot}=\Delta p\cdot V_v \tag{17}$$

$$\Delta p=p-p_v \tag{18}$$

where E_{pot} is cavitation potential energy, p and p_v represent reference and saturation pressure, and V_v represent the vapor volume. The law of potential energy change with time in the process of the collapse as the key factor in assessing the erosion intensity, the potential power density P_{pot} of bubble clusters could be obtained from,

$$P_{pot}=\frac{dE_{pot}}{dt}=(p-p_v)\cdot\frac{dV_v}{dt}+\frac{dp}{dt}\cdot V_v \tag{19}$$

$$V_v=\alpha_v\cdot V_{cell} \tag{20}$$

where α_v and V_{cell} are vapor volume fraction as well as volume of unit cell, respectively.

The Erosive Power Method (Usta & Korkut, 2019) is an erosion assessment method depends on the time derivatives with different parameters, which could be calculated as follows,

$$E_{EPM}=(p-p_v)\cdot\frac{dV_v}{dt}+\frac{dp}{dt}\cdot V_v=\frac{d\alpha_v}{dt}\cdot V_{cell}\cdot(p-p_v)+V_{cell}\cdot\alpha_v\cdot\frac{dp}{dt} \tag{21}$$

In the calculation of this work, the different flow field parameters such as the reference pressure, saturated pressure, the time derivative are captured by ANSYS CFX® version 2021R1. And the cavitation erosion zones on the blade are predicted based on above erosion assessment formula by ANSYS CFD-Post® version 2021R1.

3.5 Numerical Setup

In the simulation, the flow field characteristics are simulated by ANSYS CFX® version 2021R1, the inlet boundary is set to the Total pressure, its starting value is 101325 Pa. The outlet boundary is set to Mass Flow rate and its value is 10 m^3/h. Different cavitation conditions can be obtained by gradually reducing inlet pressure, and when change in inlet pressure results in a 3% reduction in

Table 3 Unsteady calculation values of the head for different time steps and experimental values

Time steps	1°	2°	4°	Experimental values
Head (m)	75.88	76.63	79.89	77.53

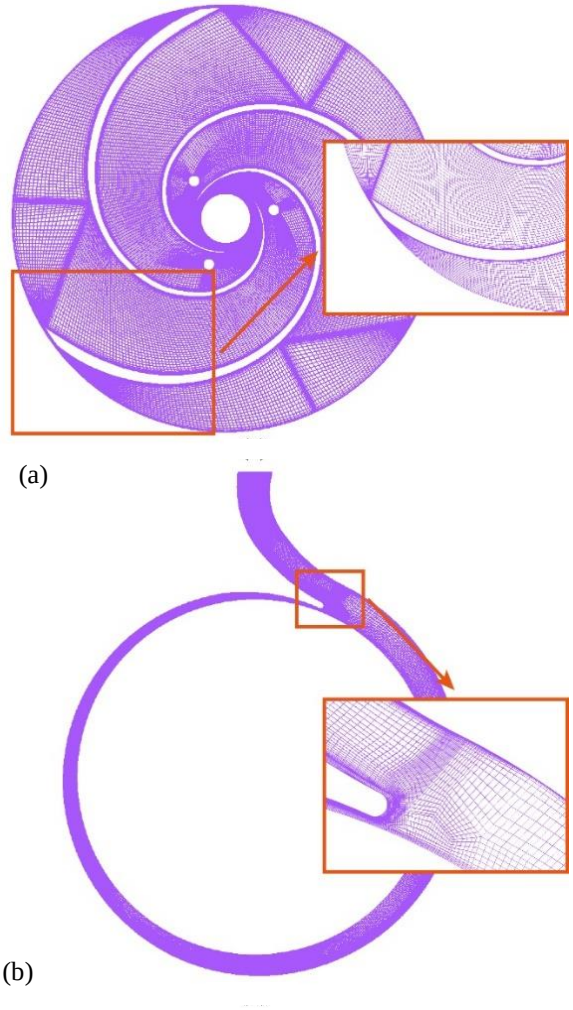

Fig. 4 Grid distribution of the computational domain, a) impeller; b) volute

condition. All walls are set to the No Slip Wall. The wall roughness is neglected based on the research (Lin et al. 2022). The impeller is set to a rotating domain which is kept at the same speed as that of the experiment, whereas the remaining components are static domains. The surfaces of the inlet section, pump chamber, and wear ring 2 connected to the impeller are set as the rotating and static intersection surfaces respectively, while the other intersection surfaces are coupled in static intersection mode. To select an appropriate time step, the head at design flow rate and critical cavitation conditions are calculated using time steps of 5.7415×10^{-5} s, 1.14943×10^{-4} s, and 2.29886×10^{-4} s, which corresponding to the rotation angles of 1°, 2°, and 4°, respectively. The average values over a rotation period is then calculated and compared to the experimental values as shown in Table 3. The time step is 1.14943×10^{-4} s for simulation in order to assure efficiency and accuracy of numerical simulation. And the convergence residual accuracy is set to 4×10^{-7} in this work.

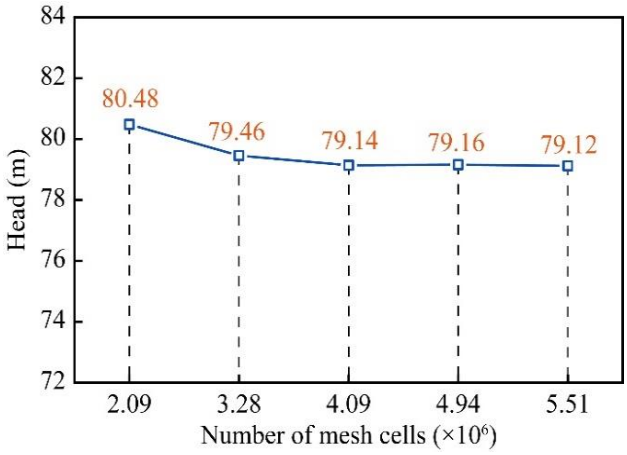

Fig. 5 Grid-independence verification

The medium employed in the present work is water at 16 °C, which has a density and saturated vapor pressure of 998.9 kg/m^3 and 1817.15 Pa, respectively.

3.6 Grid-Independent Check

A hexahedral structured mesh is used by ANSYS ICEM® version 2021R1 to assure accuracy and efficiency of calculations. The computational domain mesh is shown in Fig. 4. To account for the effect of computational domain grids on numerical calculations in the present work, a grid independence verification is conducted under the rated condition, and the head variation is used as the criterion for grid suitability. Figure 5 shows the grid-independent verification. A mesh with 4.09×10^6 cells is selected for numerical simulation based on the results of the grid verification. The optimized mesh scheme derived from the independent verification helps to mitigate the impact of the grid-related factors on the accuracy of the simulation result. To more accurately capture the flow field variations and information around the blades, the first layer height must be within a specific range. In this study, the first layer height is 0.03 mm and its grid expansion ratio is 1.5. Additionally, the y^+ value on the blade surface was kept below 30 in order to meet the requirement of turbulence model in this calculation. Figure 6 shows the distribution of y^+ values on the blade surface.

4. Results And Discussion

4.1 Validation of the Numerical Approach

The test is conducted on the original pump with a balance hole (φ = 50°) to assess the reliability of the simulation findings. A comparison curve of external characteristics of original pump at a rated speed with flow rates between 6 m^3/h and 14 m^3/h is shown in Fig. 7. Under the rated operating conditions, the test head is 79.93 m and numerical result is 79.14 m, with a relative error of less than 1%. The reason for numerical head is somewhat

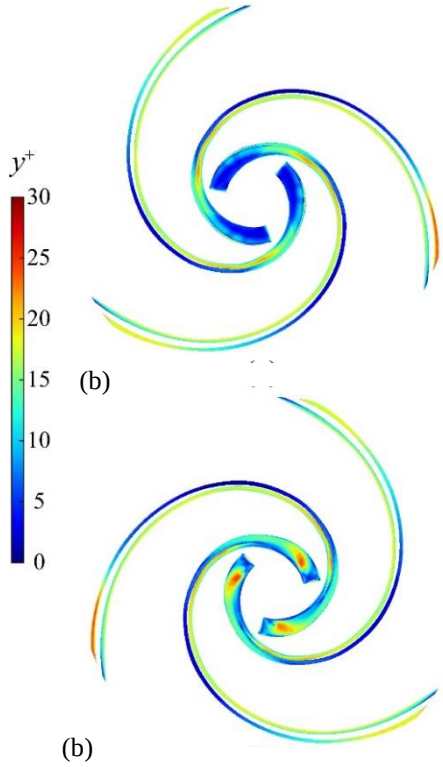

Fig. 6 Distribution of y^+ on the blade surface, a) pressure surface; b) suction surface

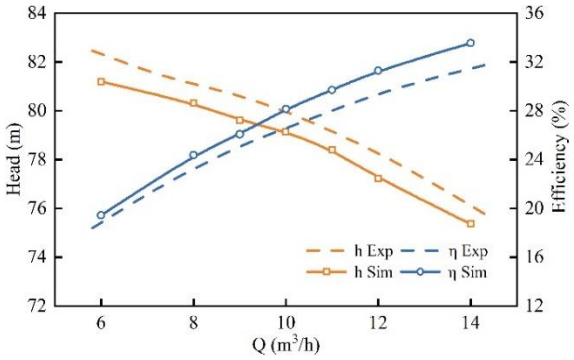

Fig. 7 Comparison of the external characteristics of the original pump (φ = 50°)

smaller than experimental head is that this simulation conditions cannot fully replicate the actual requirements of the experiment. And numerical efficiency is slightly higher than the experimental results because this calculation didn't take into account the mechanical and volumetric losses. Overall, the change in trend of the experimental head and efficiency curve can be accurately predicted by using the present numerical methods.

In addition, a comparison of the curves reveals that values of head calculated from simulation are smaller than test results, while the efficiency is higher. The trend of the simulated external characteristic curve is consistent with that obtained from the experiment. It is worth mentioning that the highest efficiency point on the original pump is not at the rated flow condition, and the efficiency steadily

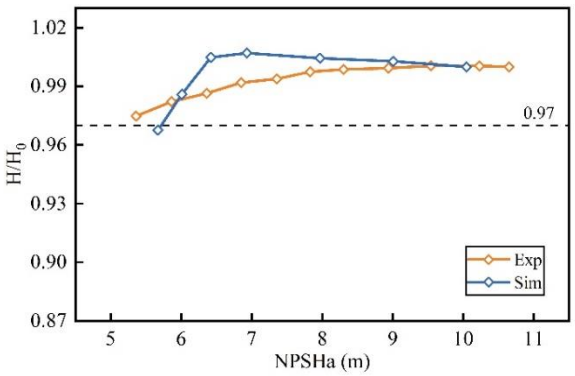

Fig. 8 Comparison of the cavitation performance of the original pump

increases as the flow rate increases. The optimal working condition shifts significantly from the design working condition primarily on account of a small geometry of this pump. The fluid viscosity effect is more pronounced, and the flow loss is greater so that the high efficiency point shifts to the high flow working condition.

A comparison between experimental and simulated cavitation behaviour curve of the original pump under rated settings is shown in Fig. 8. A vacuum pump is utilized in the experiment to evacuate the water storage tank to lower the inlet pressure at rated flow condition. The cavitation performance curve is then plotted using the head and NPSHa values for different inlet pressures, and the NPSHa can be obtained from,

$$NPSH_a = \frac{p_s}{\rho g} + \frac{v_s^2}{2g} - \frac{p_v}{\rho g} \tag{22}$$

Upon comparing the cavitation performance curves reveals, it is evident that there are minor differences between test and simulation, the curves follow the same variation pattern. The inlet pressure decreases and the head increases slightly at the beginning of the cavitation simulation. The cavitation becomes more pronounced as inlet pressure falls to a particular level, altering internal flow conditions such that the head no longer rises and begins to have a downward trend. As the inlet pressure continues to reduce, cavitation intensifies and the head-down tendency increases. The severity of pump cavitation escalates when the head reduces by approximately 3%, thereby undermining the capacity of the pump for safe and dependable operation. In general, this is regarded as a critical cavitation state and is referred to as the critical cavitation condition.

As shown in Fig. 9, the cavitation bubbles corresponding to the four typical *NPSH* are selected for evolutionary analysis to further examine the cavitation development process of the original pump. Figure 9 (a) illustrates that cavitation generates in the balance holes in the original pump during initial stage of cavitation. This is attribute to low pressure of balance holes connecting the impeller and wear ring 2, which induces the occurrence of cavitation in this region, and the pressure distribution is shown in Fig. 10, the operating pressure is the saturated vapor pressure of 1817.15Pa. In addition, the cavitation

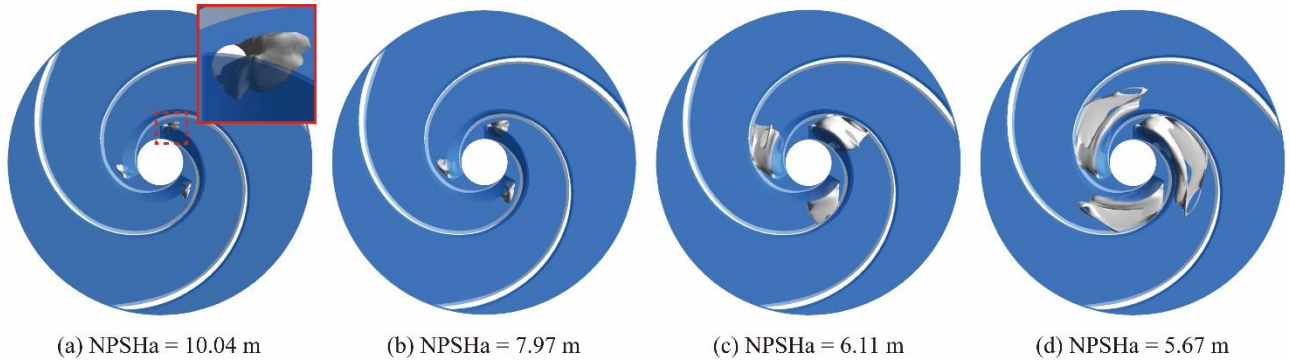

Fig. 9 Cavitation evolution of the original pump (The cavitation structure in the simulation is shown by iso-surfaces of the vapor volume fraction α_v = 0.1.)

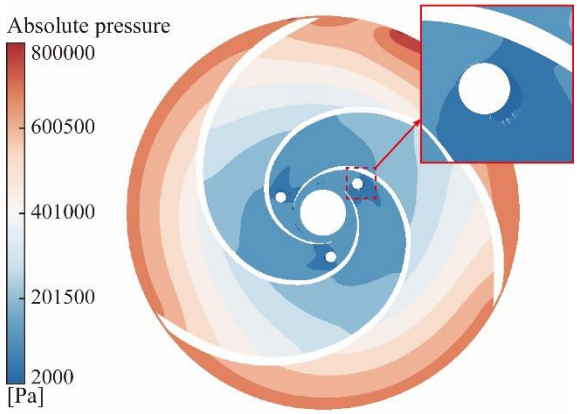

Fig. 10 Distribution of the impeller absolute pressure (NPSHa = 10.04 m)

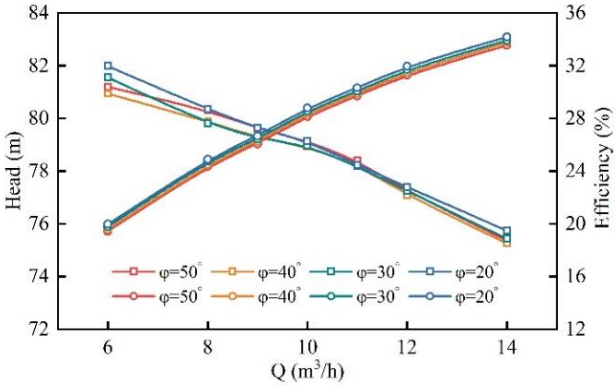

Fig. 11 Comparison of external characteristics of different schemes

induced by the balance hole has a clustered structure, which is significantly different from the attached cavitation generated at the blade suction surface. When NPSHa = 6.93 m, the cavitation of the pump becomes more noticeable, and cavitation bubbles accumulate in large numbers in the area following the balance hole. As a result, the flow field of pump is affected and its performance also begins to decline. As cavitation continues to advance, the group of cavitation bubbles proliferates across the blade surface, which causes impeller passage blockage. At the critical cavitation condition, when NPSHa = 5.67 m, increased cavitation will significantly impacting the flow state of the pump by causing blockage in its passages. It is noteworthy that the trailing of cavitation bubbles begins to move away from blade suction surfaces as a result of rotation effect of pump, accompanied by shedding of the bubbles.

It is evident from the examination of the cavitation development of the original pump described above that there is a local low pressure between balance hole and blade suction surface, which creates the objective conditions for cavitation to occur and develop. Therefore, it is necessary to increase the local pressure in the balance holes to improve its cavitation behaviour.

Then, the variation and influence mechanism of the cavitation behaviour of pump under different schemes of the circumferential position are investigated using the rotation angle as a quantitative criterion.

4.2 Comparison of the Performance of Different Schemes for the Circumferential Position of Balance Holes

A comparison of the external characteristics across different schemes for the circumferential position of balance holes is shown in Fig. 11. In this figure, a downward trend from the left to the right indicates a head curve, while the opposite trend indicates an efficiency curve. We find that the efficiency curves of each schemes have a relatively consistent trend. Moreover, as the φ decreases, the efficiency increases somewhat. There is no progressive increase in head with the change of the balance holes in the head curves. However, the head values of each scheme are generally close in flow scope from 10 to 12 m^3/h. When the flow rate deviates from this range, the deviation of the head values for each scheme increases gradually, but the maximum difference is less than 2 m.

It is crucial to compare and analyze the differences in axial force after changing the value of φ. Figure 12 compares the axial force of each scheme. Upon comparison, it is found that the axial force decreases significantly when the value of φ decreases, although the magnitude of the decrease is minimal. The maximum difference in axial force is 2.841 N or approximately 1.8%,

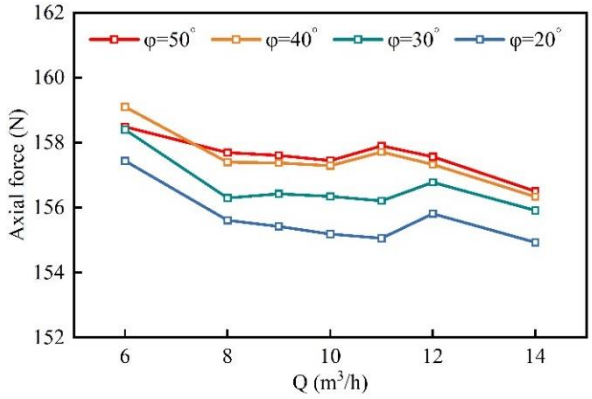

Fig. 12 Comparison of the axial forces of the rotation schemes

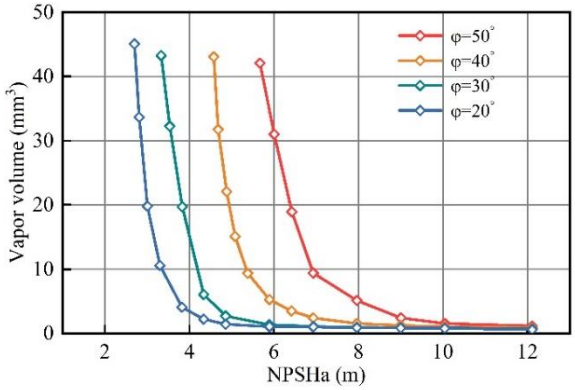

Fig. 14 Comparison of the vapor volume of the rotation schemes

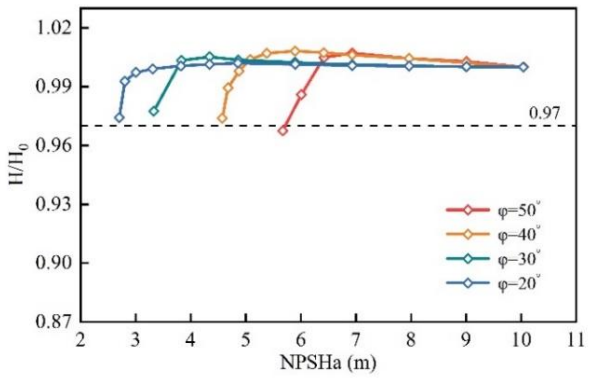

Fig. 13 Comparison of the cavitation performances of rotation schemes

so the effect of different circumferential position schemes on axial force can be negligible.

The impact of different circumferential position schemes on the cavitation behaviour is further investigated based on the above verification. Figure 13 shows comparative cavitation performance curves for various rotating balance hole schemes. It is evident that the original model (φ = 50°) has the worst cavitation performance. When NPSHa = 5.67 m, the original pump reaches the critical cavitation condition, resulting in a more pronounced head drop. For the φ= 40°, the corresponding NPSHa = 4.47 m at critical cavitation conditions. Compared with the original pump, the NPSHa is reduced by 1.1 m, which significantly improves the cavitation performance. The cavitation behaviour of pump steadily improves as the value of φ decreases. In this work, it is found that the ideal scheme for cavitation performance is achieved with a φ of 20°, and critical cavitation occurs at NPSHa = 2.7 m. It can be shown that scheme with small value of φ can enhance the cavitation behaviour.

There is a gradual decrease in behaviour of pump as the inlet pressure reduces is clearly depicted in the cavitation behaviour curve. In order to further investigate the formation of cavitation after changing φ value, the vapor volume corresponding to various balance hole rotation schemes at the corresponding inlet pressure is measured and the vapor volume change curves are shown in Fig. 14. During the change process of vapor volume, the vapor volume with a small value of φ is always less than that of the centrifugal pump with a large value of φ under the same NPSHa. As the NPSHa decreases, this phenomenon becomes more apparent.

The pump exhibits a significant increase in vapor volume when inlet pressure decreases to certain levels, resulting in a significant deterioration in cavitation performance. The scheme with the φ = 50°has the worst cavitation performance, which has a vapor volume of 9.41 mm^3 at NPSHa = 6.93 m. After reaching this point, rapidly increasing in vapor volume will gradually obstructs the flow channel, leading to a reduction in pump head. The corresponding NPSHa gradually decreases as the position of the balance hole deviates. The vapor volume increases dramatically at NPSHa = 3.3 m with the balance hole φ = 20°.

4.3 Analysis of Static Pressure on the Hub

The study indicated that by changing the value of φ, the cavitation behaviour of pump could be enhanced without compromising original head and efficiency. The distribution of static pressure on the impeller hub for various balance hole rotation schemes at rated flow condition is shown in Fig. 15. The pressure distribution on impeller hub changes as the circumferential location of balance holes varies, especially in the area near the balance holes. The area of low-pressure regions around balance holes is the largest when the value of φ is 50°. When φ = 20°, the area of low-pressure zones closest to balance holes is the smallest and nearly disappears, and the pressure distribution is more uniform.

As the balance hole connects the impeller to the wear ring 2, when fluid suddenly enters the narrower balance hole from the comparatively wide channel of the wear ring 2, a jet is formed in the balance hole, resulting in a region of low-pressure. Furthermore, low-pressure zones are easily formed near blade suction surfaces as a result of the structural characteristics of this pump, and the distribution of pressure is typically less than the pressure side. Therefore, the pressure at the balance holes increase as the balance holes move away from suction surface, and the low-pressure area near balance holes gradually decreases.

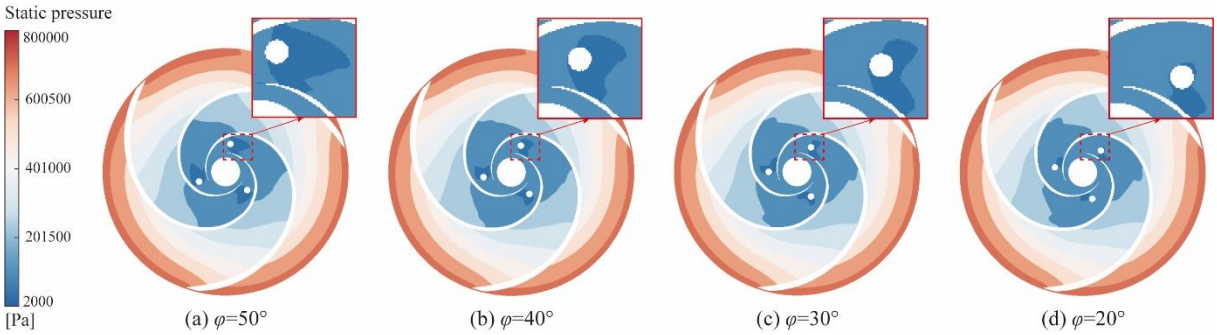

Fig. 15 Distribution of static pressure on the impeller hub

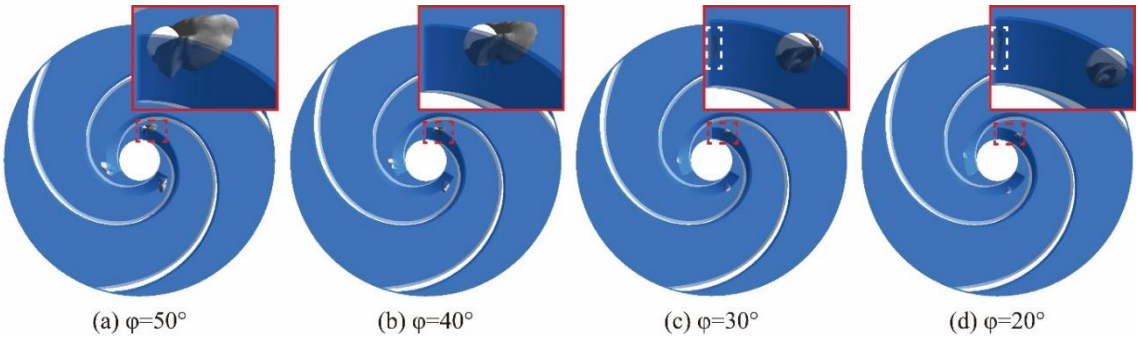

Fig. 16 Distribution of Cavitation at NPSHa = 10.04 m (The cavitation structure in the simulation is shown by iso-surfaces of the vapor volume fraction α_v = 0.1.)

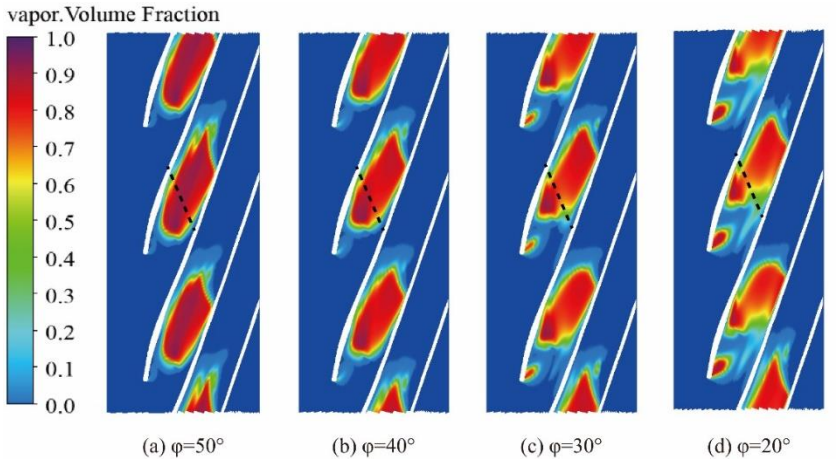

Fig. 17 Distribution of cavitation on the span=0.5 surface under critical cavitation condition

4.4 Analysis of Cavitation

Figure 16 illustrates the distribution of cavitation for different balance hole rotation schemes at NPSHa = 10.04 m. Due to the existence of balance holes, a region with low-pressure develops within it, which eventually generates cavitation. It can be found that the distribution of cavitation for different rotation schemes at the same NPSHa differs significantly. Among these, the volume of cavitation in the balance hole decreases as the value of φ reduces. This is because the pressure in the surrounding area increasing after rotating the balance hole, which in turn inhibits cavitation to some extent. As it can be shown in Fig. 16(c) and (d), cavitation is generated not only in the balance hole but also at the leading edge of blade. The cavitation incipient positions as well as distribution of pressure inside impeller change when the value of φ decreases.

Figure 17 shows the distribution of cavitation on a typical section of a blade (span = 0.5) under critical cavitation conditions corresponding to various balance hole rotation schemes. At the critical cavitation condition, the cavitation pattern in the section varies significantly. As the value of φ reduces, the cavitation in the section shows a tendency to collapse, as shown by dashed black lines in this figure. And the proportion of higher vapor volume fraction in the cavitation core region decreases, indicating that the cavitation in pump with larger value of φ is more severe. When the value of φ is 50°, the development of cavitation in pumps is completely dominated by the balance hole, and even under the critical cavitation

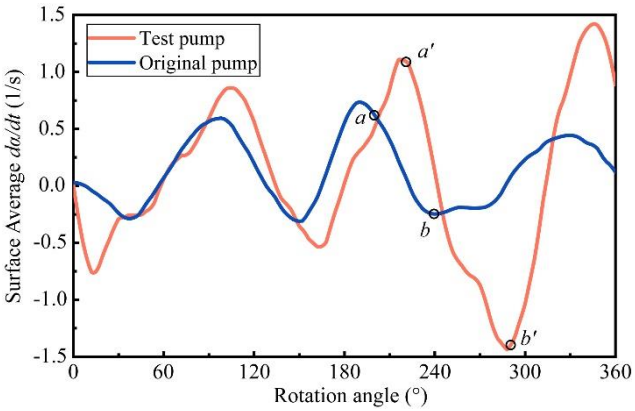

Fig. 18 Variation of the time derivative of the vapor volume fraction ($d\alpha / dt$) in a single rotation period of a typical blade

condition, there is no visible cavitation appear near the front of blade. The cavitation in the zone close to leading edge becomes increasingly noticeable as the value of φ decreases. At φ = 20°, the cavitation in this zone is significant, with the vapor volume fraction in its internal core area reaching 0.9, indicating that cavitation has completely formed.

4.5 Prediction of Cavitation Erosion on Blade

According to the aforementioned cavitation study, the scheme with the value of φ is 20° exhibited the best cavitation performance. In this section, the Erosive Power Method for calculating cavitation erosion at centrifugal pump blades is employed to compare the erosion intensity of the test pump (φ = 20°) with that of the original pump (φ = 50°) and analyze erosion mechanism.

Figure 18 shows the time derivative of the vapor volume fraction ($d\alpha / dt$) variation comparison between the original pump (φ = 50°) and the test pump (φ = 20°) during a single rotation period of a typical blade. The observation highlights that the properties of the blade surface parameters in a centrifugal pump change over time during rotation. The fluctuation range of the $d\alpha / dt$ is wider after altering circumferential positions of balance holes, indicating that the instantaneous changes in bubbles growth and collapse on blade surfaces are more noteworthy. Two moments *a* and *b* of the original pump curve and two moments *a′* and *b′* of the test pump curve are chosen as representatives for further investigation of the erosion parameter distribution of the blade surface to better understand the cavitation erosion.

Figures 19 and 20 show the variation of the $d\alpha / dt$ on different blade spans of a typical blade at typical

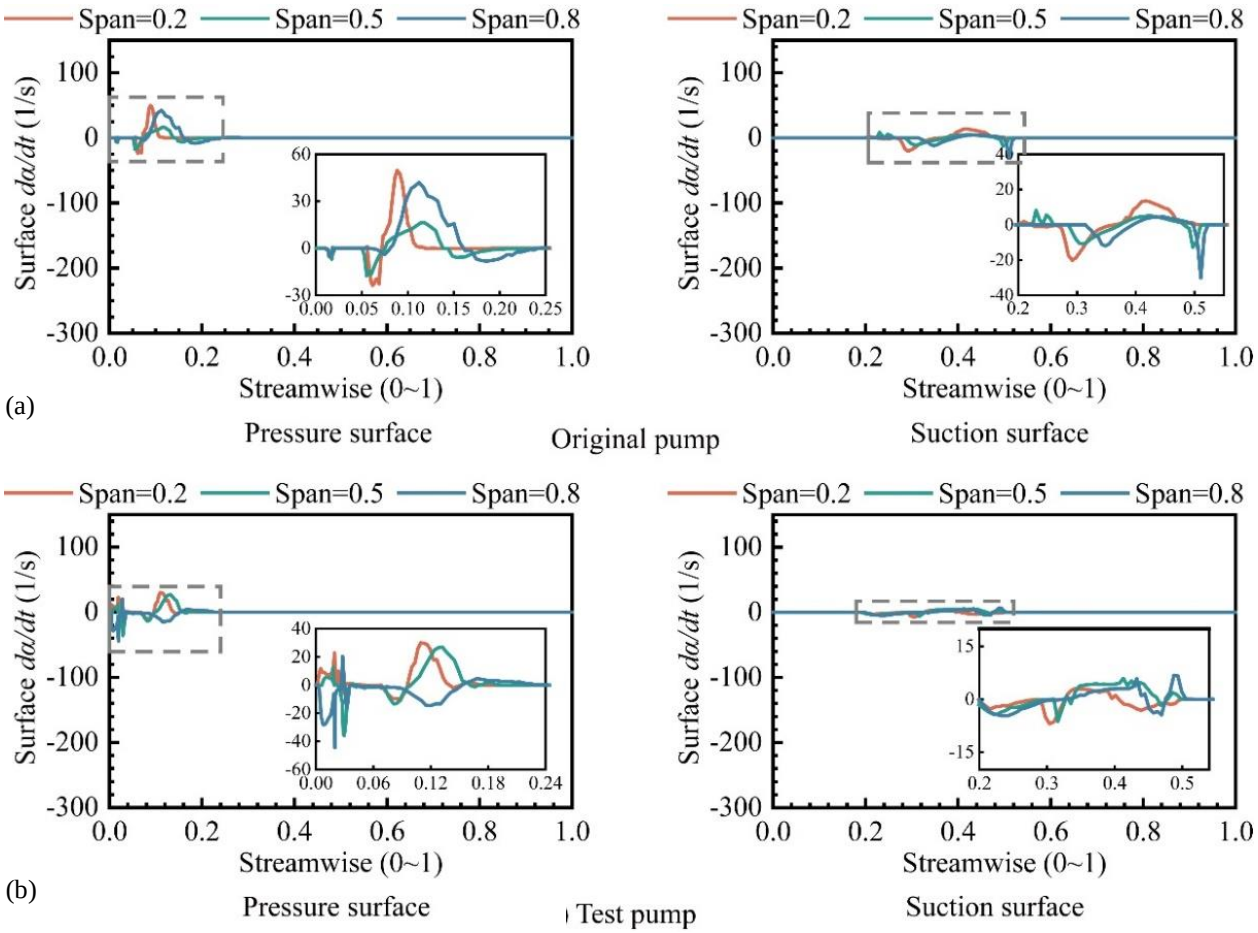

Fig. 19 Comparison of $d\alpha / dt$ on different blade spans of a typical blade (The original pump is at moment *a*, the test pump is at moment *a′*)

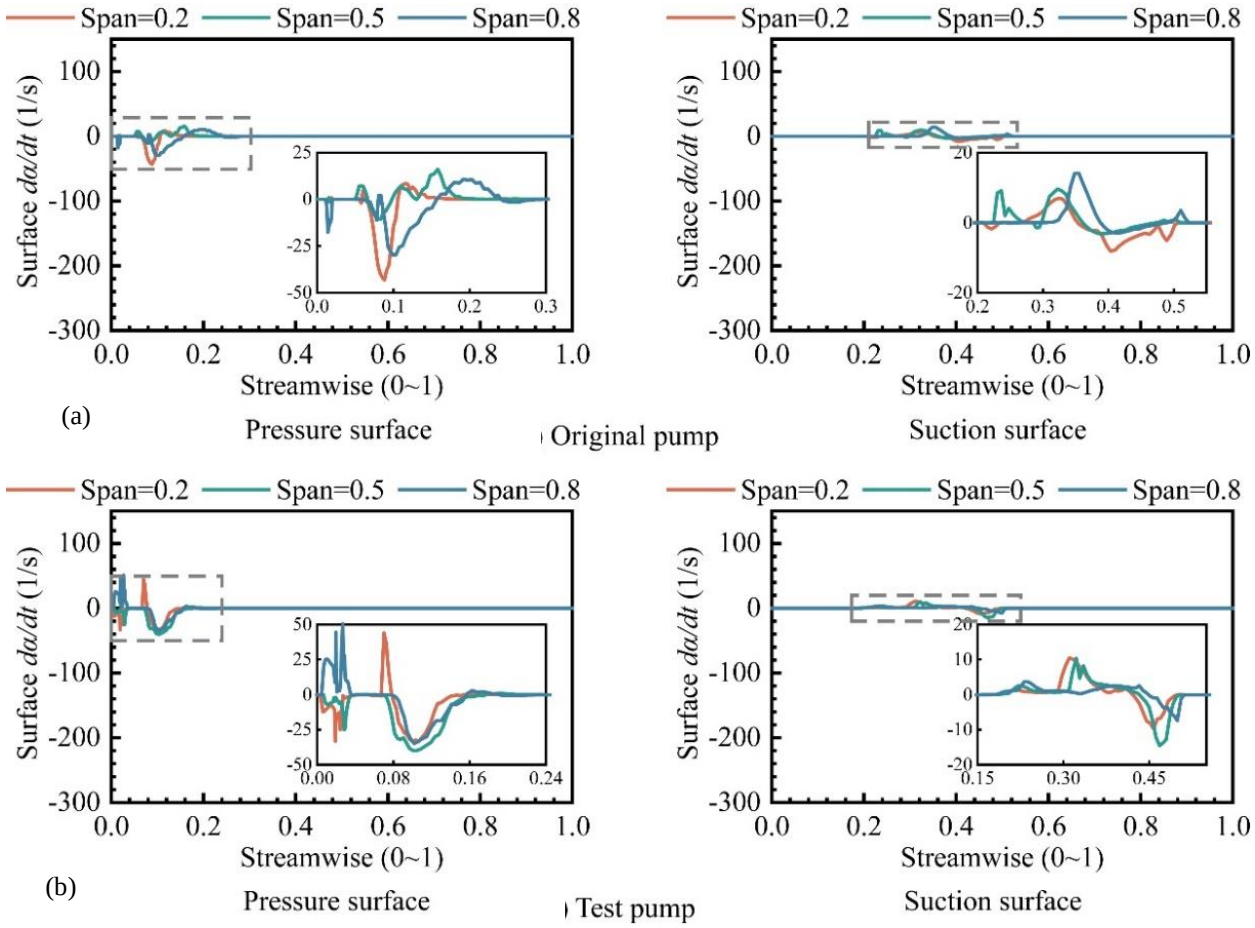

Fig. 20 Comparison of $d\alpha/dt$ on different blade spans of a typical blade (The original pump is at moment *b*, the test pump is at moment *b′*)

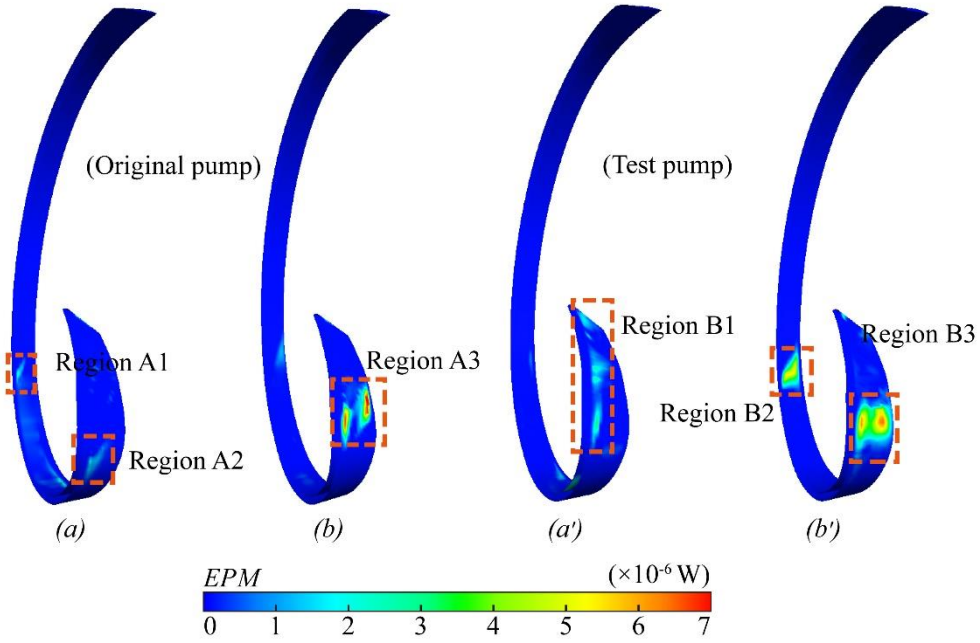

Fig. 21 Comparison of the distribution of cavitation erosion on a typical blade at different moments

moments. According to the $d\alpha/dt$ curve, the positive value of $d\alpha/dt$ indicates that the cavitation is in the growth phase, while a negative value suggests that the cavitation is collapsing. According to the selected moments, the *a* and *a′* represent cavitation growth, while the *b* and *b′* moments represent the collapse of cavitation. Comparing the different changing pattern in $d\alpha/dt$ on the suction and pressure surfaces, it can be found that the

original pump exhibits more significantly variation both on the suction and pressure surfaces, while the test pump demonstrates more significant changes on the pressure surface. According to the structure of this pump, it is evident that the positions of balance holes in the test pump are nearer to the pressure surface, which results in a more pronounced influence of cavitation on pressure surfaces. As a result, there is a significant difference between the original pump and the test pump in the distribution of the value of $d\alpha/dt$. The variation curves indicate that for both the original pump and the test pump, the positions on the pressure surface where cavitation transient changes near the leading edge of blades. However, those positions on the suction surface of both are primarily located at the midsection of the blade, while for the test pump these positions are relatively more rearward. Comparing the amplitude of variation for $d\alpha/dt$ shows that the change in the vapor volume fraction is more significantly in the original pump, thereby indicating a more significant cavitation fluctuation in the original pump.

To further investigate erosion difference on the blade surfaces, predictions of erosion regions on a typical blade are conducted for the aforementioned moments using the EPM as shown in Fig. 21. The zones of high erosion danger are found at the positions where the cavitation is about to separate from the blade surface such as regions A3 and B3. This is due to the considerable and continuous energy impact on the blade resulting from the collapse of numerous cavitation structures as the cavitation separates from the blade in this region. These results agree well with the previously discussed variation trend of the $d\alpha/dt$ curves on the pressure surfaces. The figure shows that the small-scale erosion regions observed in region A1 of the original pump and region B2 of the test pump corresponds to the stages of cavitation collapse as indicated by the $d\alpha/dt$ curves on the suction surfaces. A comparison of regions A3 and B3 shows that even though region B3 has a larger erosion area, its erosion intensity is significantly lower than region A3. As a result, the test pump ameliorates the erosion intensity in zones with high erosion danger, especially beside the leading edge of blade close to inlet.

5. CONCLUSION

In this work, numerical method is employed to simulate the flow field of a centrifugal pump, in particular to investigate the laws of change in internal flow field characteristics and impact of circumferential positions of balance holes on cavitation behaviour and cavitation erosion. The conclusions may be summarized as follows:

(1) After rotating circumferential positions of balance holes, the efficiency slightly increases as the φ value decreases. The head of this pump under various schemes is closer in the flow range from 10 - 12 m^3/h. As the flow deviates from this range, the deviation of the head gradually increases, but the impact on the external characteristics is not significant.

(2) Utilizing balance hole allows the high pressure liquid in a balance chamber to increase the pressure on suction surface, effectively suppressing cavitation. In the present work, the axial force decreases significantly when the value of φ decreases, although the magnitude of the decrease is minimal. The maximum difference in axial force is 2.841 N or approximately 1.8%.

(3) The original pump described in this work generates cavitation in the balance hole at lower pressure, which subsequently grows and eventually obstructs the flow passage. The cavitation behaviour of this centrifugal pump is improved as φ value decreases and the area of the low-pressure region around the balance hole gradually decreases.

(4) The critical cavitation pattern shows a tendency to collapse as the value of φ reduces. Additionally, the proportion of higher vapor volume fraction in the cavitation core region decreases as a result of this trend, indicating that the cavitation is more severe in centrifugal pumps with a bigger balance hole angle.

(5) The Erosive Power Method can well predict the zones and intensity of cavitation erosion on the blade surface. The erosion intensity on blade surface of original pump is significantly higher than test pump with a φ of 20° under the critical cavitation conditions, resulting in more pronounced damage to the blade material. The scheme with a φ of 20° improves the cavitation behaviour of this centrifugal pump. As a consequence, it reduces the intensity of cavitation erosion to a certain extent.

ACKNOWLEDGEMENTS

This study is supported by the National Natural Science Foundation of China (No. 51806082), the Science and Technology Support Program of Taizhou City (No. TG202320), Open Research Subject of Key Laboratory of Fluid and Power Machinery (Xihua University), Ministry of Education (No. LTDL-2023009).

CONFLICT OF INTEREST

The authors declare that they have no known competing financial interests or personal relationships that could have appeared to influence the work re-ported in this paper.

AUTHORS CONTRIBUTION

Doubin Xun: Investigation, Formal analysis, Methodology, Software, Validation, Data curation, Writing - original draft. **Ning Qiu:** Investigation, Conceptualization, Project administration, Resources, Visualization, Writing - review & editing, Funding acquisition, Supervision. **Yangyang Wei:** Methodology, Data curation, Visualization. **Han Zhu:** Investigation, Methodology, Writing - review & edit-ing. **Wenjie Zhou:** Formal analysis, Writing - review & editing, Supervision. **Pei Xu:** Methodology, Soft-ware, Writing - review & editing. **Weibin Zhang:** Investigation, Methodology.

REFERENCES

Aktas, B., Atlar, M., Fitzsimmons, P., & Shi, W. (2018).

An advanced joint time-frequency analysis procedure to study cavitation-induced noise by using standard series propeller data. *Ocean Engineering, 170*, 329-350. https://doi.org/10.1016/j.oceaneng.2018.10.026

Arabnejad, M. H., Svennberg, U., & Bensow, R. E. (2021). Numerical assessment of cavitation erosion risk using incompressible simulation of cavitating flows. *Wear, 464*, 203529. https://doi.org/10.1016/j.wear.2020.203529

Brennen, C. E. (2011). *Hydrodynamics of pumps*. Cambridge University Press. https://doi.org/10.1017/CBO9780511976728

Cao, W., Yang, X., & Jia, Z. (2022). Numerical simulation of cavitation flow in a low specific-speed centrifugal pump with different diameters of balance holes. *Journal of Marine Science and Engineering, 10*(5), 619. https://doi.org/10.3390/jmse10050619

Chen, Z. X., Hu, H. X., Guo, X. M., & Zheng, Y. G. (2022). Effect of groove depth on the slurry erosion of V-shaped grooved surfaces. *Wear, 488*, 204133. https://doi.org/10.1016/j.wear.2021.204133

Cheng, X., Chang, Z., & Jiang, Y. (2020). Study on the influence of the specific area of balance hole on cavitation performance of high-speed centrifugal pump. *Journal of Mechanical Science and Technology, 34*, 3325-3334. https://doi.org/10.1007/s12206-020-0725-z

Cui, B. L., Han, X. T., & An, Y. T. (2022). Numerical simulation of unsteady cavitation flow in a low-specific-speed centrifugal pump with an inducer. *Journal of Marine Science and Engineering, 10*(5), 630. https://doi.org/10.3390/jmse10050630

Dular, M., Stoffel, B., & Širok, B. (2006). Development of a cavitation erosion model. *Wear, 261*(5-6), 642-655. https://doi.org/10.1016/j.wear.2006.01.020

Fortes Patella, R., & Reboud, J. L. (1998). A new approach to evaluate the cavitation erosion power. https://doi.org/10.1115/1.2820653

Gangipamula, R., Ranjan, P., & Patil, R. S. (2022). Study on fluid dynamic characteristics of a low specific speed centrifugal pump with emphasis on trimming operations. *International Journal of Heat and Fluid Flow, 95*, 108952. https://doi.org/10.1016/j.ijheatfluidflow.2022.108952

Gao, B., Guo, P., Zhang, N., Li, Z., & Yang, M. (2017). Experimental investigation on cavitating flow induced vibration characteristics of a low specific speed centrifugal pump. *Shock and Vibration, 2017*. https://doi.org/10.1155/2017/6568930

Haosheng, C., Jiang, L., Darong, C., & Jiadao, W. (2008). Damages on steel surface at the incubation stage of the vibration cavitation erosion in water. *Wear, 265*(5-6), 692-698. https://doi.org/10.1016/j.wear.2007.12.011

Hu, Q. X., Yang, Y., & Shi, W. D. (2020). Cavitation simulation of centrifugal pump with different inlet attack angles. *International Journal of Simulation Modelling, 19*(2), 279-290. https://doi.org/10.2507/ISIMM19-2-516

Huang, M., Kim, K., & Suh, S. H. (2018). Numerical and experimental investigation of cavitation flows in a multistage centrifugal pump. *Journal of Mechanical Science and Technology, 32*(3), 1071-1078. https://doi.org/10.1007/S12206-018-0209-6

Köksal, Ç. S., Usta, O., Aktas, B., Atlar, M., & Korkut, E. (2021). Numerical prediction of cavitation erosion to investigate the effect of wake on marine propellers. *Ocean Engineering, 239*, 109820. https://doi.org/10.1016/j.oceaneng.2021.109820

Li, L. M., Wang, Z. D., Li, X. J., Wang, Y. P., & Zhu, Z. C. (2021). Very large eddy simulation of cavitation from inception to sheet/cloud regimes by a multiscale model. *China Ocean Engineering, 35*(3), 361-371. https://doi.org/10.1007/s13344-021-0033-0

Li, L., Pei, C., Wang, Z., Lin, Z., Li, X., & Zhu, Z. (2024). Assessment of cavitation erosion risk by Eulerian–Lagrangian multiscale modeling. International *Journal of Mechanical Sciences, 262*, 108735. https://doi.org/10.1016/j.ijmecsci.2023.108735

Li, Z. R., Pourquie, M., & Van Terwisga, T. (2014). Assessment of cavitation erosion with a URANS method. *Journal of Fluids Engineering, 136*(4), 041101. https://doi.org/10.1115/1.4026195

Lin, Y., Li, X., Zhu, Z., Wang, X., Lin, T., & Cao, H. (2022). An energy consumption improvement method for centrifugal pump based on bionic optimization of blade trailing edge. *Energy, 246*, 123323. https://doi.org/10.1016/j.energy.2022.123323

Luo, X. W., Ji, B., & Tsujimoto, Y. (2016). A review of cavitation in hydraulic machinery. *Journal of Hydrodynamics, 28*(3), 335-358. https://doi.org/10.1016/S1001-6058(16)60638-8

Luo, X., Xie, H., Feng, J., Ge, Z., & Zhu, G. (2022). Influence of the balance hole on the performance of a gas–liquid two–phase centrifugal pump. *Ocean Engineering, 244*, 110316. https://doi.org/10.1016/j.oceaneng.2021.110316

Luo, X., Zhang, Y., Peng, J., Xu, H., & Yu, W. (2008). Impeller inlet geometry effect on performance improvement for centrifugal pumps. *Journal of mechanical science and technology, 22*, 1971-1976. https://doi.org/10.1007/s12206-008-0741-x

Melissaris, T., Schenke, S., Bulten, N., & van Terwisga, T. J. (2020). On the accuracy of predicting cavitation impact loads on marine propellers. *Wear, 456*, 203393. https://doi.org/10.1016/j.wear.2020.203393

Peters, A., Sagar, H., Lantermann, U., & el Moctar, O. (2015). Numerical modelling and prediction of cavitation erosion. *Wear, 338*, 189-201. https://doi.org/10.1016/j.wear.2015.06.009

Usta, O., & Korkut, E. (2019). Prediction of cavitation development and cavitation erosion on hydrofoils and propellers by detached eddy simulation. *Ocean*

Engineering, *191*, 106512. https://doi.org/10.1016/j.oceaneng.2019.106512

Wang, D. W., Liu, Z. L., Han, W., & Fu, Y. (2021). Effect of adjusting balance hole to cavitation area on cavitation performance of a centrifugal pump. *International Journal of Fluid Machinery and Systems*, *14*(3), 289-299. https://doi.org/10.5293/IJFMS.2021.14.3.289

Wang, W. T., Lu, H., & Meng, G. Q. Q. G. (2018, July). *Pressure fluctuation characteristics induced by cavitation in a centrifugal pump* [Conference session]. Asian Working Group- IAHR's Symposium on Hydraulic Machinery and Systems, Beijing, China. https://doi.org/10.1088/1755-1315/163/1/012040

Wang, Z., Cheng, H., Bensow, R. E., Peng, X., & Ji, B. (2023). Numerical assessment of cavitation erosion risk on the Delft twisted hydrofoil using a hybrid Eulerian-Lagrangian strategy. *International Journal of Mechanical Sciences*, *259*, 108618. https://doi.org/10.1016/j.ijmecsci.2023.108618

Wang, Z., Li, L., Li, X., & Zhu, Z. (2022, April). *Numerical simulation of cavitating flow around a twist hydrofoil focusing on the erosion behaviour*. Journal of Physics: Conference Series (Vol. 2217, No. 1, p. 012011). IOP Publishing. https://doi.org/10.1088/1742-6596/2217/1/012011

Wei, Y., Yang, Y., Zhou, L., Jiang, L., Shi, W., & Huang, G. (2021). Influence of impeller gap drainage width on the performance of low specific speed centrifugal pump. *Journal of Marine Science and Engineering*, *9*(2), 106. https://doi.org/10.3390/jmse9020106

Yin, T., Pavesi, G., Pei, J., & Yuan, S. (2021). Numerical investigation of unsteady cavitation around a twisted hydrofoil. *International Journal of Multiphase Flow*, *135*, 103506. https://doi.org/10.1016/j.ijmultiphaseflow.2020.103506

Zhang, J., Li, G., Mao, J., Yuan, S., Qu, Y., & Jia, J. (2018). Effects of the outlet position of splitter blade on the flow characteristics in low-specific-speed centrifugal pump. *Advances in Mechanical Engineering*, *10*(7), 1687814018789525. https://doi.org/10.1177/1687814018789525

Zhao, J. J., Mu, J. G., Zheng, S. H., Lu, H. Q., & Wang, H. (2012). The impact of balance hole radial position of centrifugal pump on axial force and external characteristics. *Applied Mechanics and Materials*, *130*, 1691-1695. https://doi.org/10.4028/www.scientific.net/AMM.130-134.1691

Zhao, W., Yu, J., Xu, Y., Xu, Z., & Wang, G. (2020). Effect of hub-fitted tiny blade in centrifugal pump on cavitation suppression. *Journal of Harbin Engineering University*, *41*(12), 1827-1833. http://doi.org/10.11990/jheu.201905025

Zhu, B., & Chen, H. X. (2012). Cavitating suppression of low specific speed centrifugal pump with gap drainage blades. *Journal of Hydrodynamics*, *24*(5), 729-736. https://doi.org/10.1016/S1001-6058(11)60297-7

Zhu, H., Qiu, N., Wang, C., Si, Q., Wu, J., Deng, F., & Liu, X. (2021). Prediction of cavitation evolution and cavitation erosion on centrifugal pump blades by the DCM-RNG method. *Scanning*, *2021*. https://doi.org/10.1155/2021/6498451

Zwart, P. J., Gerber, A. G., & Belamri, T. (2004, May). *A two-phase flow model for predicting cavitation dynamics.* Fifth international conference on multiphase flow (Vol. 152). Yokohama, Japan.